Acta Scientiarum
http://periodicos.uem.br/ojs
ISSN on-line: 1807-8664
Doi: 10.4025/actascitechnol.v44i1.60535

GUI-CAD Tool to assist the multiclass classification of mammary pathologies by infrared images

Kamila Fernanda Ferreira da Cunha Queiroz[1*], Marcus Costa Araújo[2], Hugo Dourado[3] and Rita de Cássia Fernandes de Lima[2]

[1]Diretoria Acadêmica de Ciências, Instituto Federal de Educação, Ciência e Tecnologia do Rio Grande do Norte, BR-406, Km 145, 59570-000, Bairro Planalto, Ceará-Mirim, Rio Grande do Norte, Brasil. [2]Departamento de Engenharia Mecânica, Universidade Federal de Pernambuco, Recife, Pernambuco, Brasil. [3]Institute for Computational Cell Biology, Heinrich-Heine-Universität Düsseldorf, Düsseldorf, Germany. *Author for correspondence: E-mail: kamilafqueiroz@gmail.com

ABSTRACT. Infrared thermography is a potential method to improve efficiency for early detection of breast cancer. This technique does not use ionizing radiation and is feasible for screening in men and for detecting changes in young women. In this study, ninety-eight infrared images were used to create a database to develop a computer-aided diagnosis system. Typically, this kind of system is associated with graphical interfaces to facilitate users' work. In this study, the computer-aided diagnosis was implemented based on statistical classifiers for analysis of four classes: Malignant Tumor, Benign Tumor, Cyst and Healthy. The region of interest was segmented in automatic and semiautomatic ways, which is respectively associated with the Support Vector Machine classifier and Mahalanobis classifier. To evaluate the performance of the proposed classifiers, a confusion matrix was applied to each result obtained. Using the proposed GUI-CAD tool, it was possible to carry out individual and unsupervised classification of patients, with 93% sensitivity.

Keywords: Breast lesion; breast cancer; thermography; computer-aided diagnosis; user-computer interface.

Received on August 12, 2021.
Accepted on December 6, 2021.

Introduction

Breast cancer is a major public health problem. It is the most common malignancy in women in most of the world. The Global Cancer Observatory, published in 2021, estimates 2.3 million new cases of breast cancer and 685 thousand deaths from the disease (Sung et al., 2021). In <omit>, estimates of breast cancer incidence for each year of the 2020-2022 triennial are 66,280 new cases. Disregarding non-melanoma skin tumors, female breast cancer occupies the first most frequent position in all regions of the country (Instituto Nacional de Câncer José Alencar Gomes da Silva [INCA], 2019).]

Some techniques are used to screen breast cancer early and this detection is essential for successful treatment. Mammography is the main screening method to diagnose this type of cancer. However, this technique can be ineffective for women with fibrocystic breasts, dense breasts, or surgically implanted breasts. Addition to, ionizing radiation is emitted and there is a discomfort caused by the compression of the breasts between flat surfaces to improve the image quality (Duffy et al., 2020).

Thus, the adoption of additional diagnostic methods, such as thermography, can be important to increase the efficiency to detect breast cancer earlier (Singh & Singh, 2020). It is known that temperatures of breast tissue with some types of abnormality are higher than temperatures of normal tissues (Acharya, Ng, Sree, Chua, & Chattopadhyay, 2014). The thermographic camera can measure this increase in temperature on the breast surface.

Due to the limitation of the human visual system and the lack of experience in interpretation of medical images, Computer-Aided Diagnosis (CAD) systems were developed to improve the detection of abnormalities in distinct areas of medicine. An accurate statistical classifier is the most important component of any CAD system that can be developed. The use of a CAD system based on thermographic images may represent a powerful tool that aid the diagnosis of breast cancer (Araújo, Souza, Lima, & Silva Filho, 2017). Using temperatures measured, it is possible to analyze patients without breast abnormalities, and patients with malignant tumor, benign tumor, or cyst.

Interpretation is a repetitive task that requires attention to details. On the other hand, objective image analysis, such as thermograms, performed by automated systems, provides consistent performance, but its accuracy is usually low. Due to the importance of this problem, specialists should be involved because computers cannot replace them completely. However, computer systems can help them to achieve the best analyses.

CAD systems are usually associated with graphical interfaces to facilitate users' work. One of the main advantages of creating a graphical user interface (GUI) is to make the developed computation program accessible to a person who does not know the programming language (Kapoor, Prasad, & Patni, 2012; Ekici & Jawzal, 2020). In this context, thermography in conjunction with CAD systems, can have great potential in diagnosing breast abnormalities using thermograms.

In this context, the objective of this study was to develop a new screening tool capable of diagnosing the main breast changes, especially breast cancer. A graphic interface was developed to allow the researcher or the physician to simply and quickly evaluate a breast abnormality using thermographic images.

Related works

Most works on breast cancer diagnosis using infrared images (IR) images aim at binary classification of the sample, different from the initial approach of this paper. In the literature on the multi classification of IR breast images, Araújo, Lima, and Souza (2014) proposed a system for classifying breast abnormalities (malignant tumor, benign tumor, and cyst). He was used a breast thermography dataset with 50 patients. The segmentation of the breast region was performed using ellipsoidal elements semi-automatically generated by the Matlab® software. Then, a morphological process was performed on each image obtained from segmentation, which included the definition of a structuring element and erosion, dilation, and Top Hat processes, to determine the height of the maximum local temperature in relation to the temperature of its vicinity. The extraction of features was performed on matrices resulting from segmentation and morphological process and were based on temperature range data. The learning step considers the internal variation of the intervals when describing breast abnormalities and uses the Fisher's discretion to map these intervals into a space where they can be more easily separated. The classification step is based on a parameterized Mahalanobis distance for interval-valued data. Two scenarios were evaluated: the first scenario focuses on the overall misclassification rate and achieves 16 % misclassification rate and 93 % sensitivity to the malignant class. The second scenario maximizes the sensitivity to the malignant class, reaching 100 % sensitivity to this specific class and 20 % overall misclassification rate.

Dourado Neto (2014) developed a CAD system based on automatic segmentation of the breast region. For this, the temperature matrix associated with each thermographic image was treated in grayscale. These authors tested 234 patients, including 43 with cancer, 79 with benign tumor, 42 with cyst and 70 without abnormalities, among them interval features and statistics features. The most relevant pair of characteristics was determined using the WEKA software (Waikato Environment for Knowledge Analysis). The best classification method was determined by testing five supervised learning methods present in the Statistics Toolbox™ of MATLAB® 2013b: Classification Tree, Support Vector Machine, Discriminant Analysis, Naïve Bayes, and K-Nearest Neighbors. In each case, parameters were tested to achieve the best result. For the Classification Tree method, we used the MinParent parameter equal to one quarter of the total set. For the Support Vector Machine method, we used a polynomial kernel of order 7. For the Discriminant Analysis method, we used the Mahalanobis distance. For the Naïve Bayes method, we used a kernel distribution. For K-Nearest Neighbors method, also the Mahalanobis distance. The chosen method to validate the results was the leave-one-out cross-validation. For the best characteristics, the Support Vector Machine (SVM) was the most suitable classifier with 89.36% accuracy, 87.50% sensitivity and 90.32% specificity.

Ahmed, Ali, and Selim (2019) evaluated a database of 287 thermograms of patients considered healthy, benign tumor and malignant tumor. The SVM classifier showed the best result with 97.14% accuracy, 98% sensitivity and 98.60% specificity.

Vasconcelos, Santos, and Lima (2018) classified the patients as healthy, cyst, benign tumor, or malignant tumor (four classes). The best result was an accuracy of 63.46%, sensitivity of 80.77% and specificity of 86.54%, using the Sequential Minimal Optimization (SMO) classifier.

In another study, Santana et al. (2018) used 1052 images of cysts, benign tumors, and malignant tumors. Extreme Learning Machines (ELM) networks proved to be quite efficient classifiers with results indicating a sensitivity of 78% and specificity of 88%.

Rodrigues et al. (2019) proposed a multi class classification of thermographic images in a dataset of 336 images with cystic lesion, benign lesions, malignant lesions, or no lesion. Their method achieved 91.12% accuracy for the SVM classifier with exponent polynomial kernel 4.

Material and methods

In this section, the steps used to build a computational tool for breast thermographic image analysis are explained. For the development of this tool, CAD systems created by Araújo et al. (2014) and Dourado Neto (2014) were used as a basis. However, two essential changes were made: inclusion of the Healthy class in the database, increasing the universe of evaluation. An implementation of a hybrid classification system (supervised and unsupervised) for individual patient assessment was also considered. The proposed method is illustrated in Figure 1.

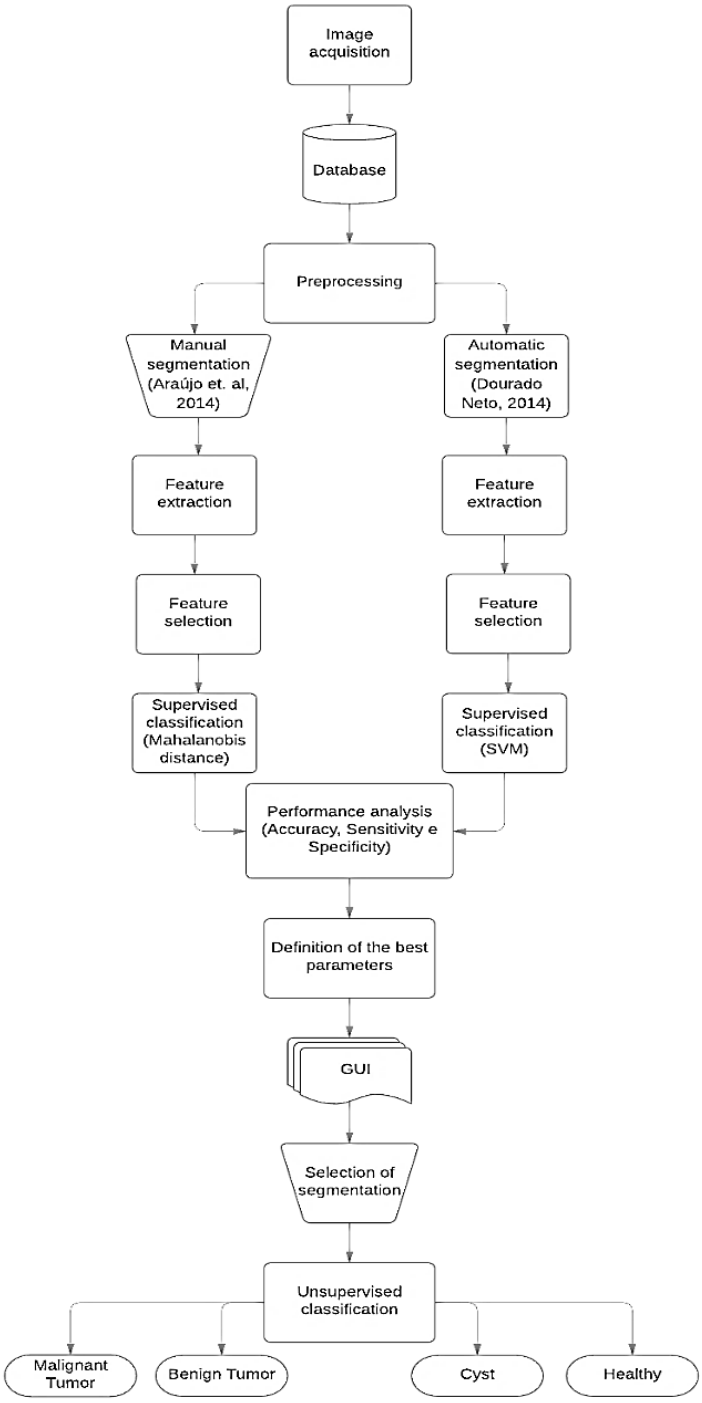

Figure 1. Flowchart of the methodology proposed.

Infrared image acquisition

Infrared (IR) or thermographic images used in this study were obtained with a FLIR S45 infrared camera. The images belong to patients followed up at the Mastology Outpatient, Hospital <omit>. The selected sample (size n = 98) was composed of an outpatient demand of women with diagnoses confirmed by clinical examination, ultrasound, mammography, and biopsy exams. Each woman agreed to participate in this research by signing an Informed Consent, a document associated with the registration of the project at the Ministry of Health (<omit>) and approved by the <omit> Ethics Committee.

A protocol for thermographic examination was adopted to reduce some errors generated by temperature variations inside the room or by the temperature of the patient during image acquisition. To standardize the referred acquisition, a mechanical apparatus to assist the correct position of the patient was used (Bezerra et al., 2013).

This apparatus (Figure 2) consists of two rails positioned on the floor that supports a small car upon which the thermographic camera and its tripod are positioned. There is a swivel chair with adjustable horizontal bars. The bars serve as a support for the patient's hands during the acquisition of some images.

Figure 2. Mechanical apparatus used in the thermographic image capture protocol.

Before image acquisition, the patient should rest around ten minutes to stabilize their temperature. In this, a sample of 98 thermograms (20 healthy subjects, 27 patients with benign tumors, 27 patients with malignant tumors and 24 patients with cyst) was used.

Breast segmentation

Considering the proposed GUI, the extraction of the region of interest (ROI) can be done manually or automatically. The automatic segmentation is performed without human intervention and usually is faster and provides greater objectivity in the final analysis. Although the speediness, the result can be unsatisfactory. Normally, manual segmentation is used to reduce segmentation errors that can appear in the automatic segmentation due to the natural asymmetry of the breasts. In addition, it allows the healthcare professional to define the best area of interest (Araújo et al., 2014).

For automatic segmentation, temperature matrices had to be treated as grayscale images, with lighter shades indicating higher temperatures. Since temperatures are accurate to two decimal places, the 8-bit (256 shades of gray) representation was not sufficient, so 16-bit images (65,536 shades of gray) were used. Images have been equalized for easy viewing. The process described in this topic is detailed in Dourado Neto (2014).

Segmentation of the temperature matrix began when the region of the patient's body was separated from the colder background. This was done by identifying the threshold value of temperature in the histogram, which separates the two regions. Then, the regions immediately below the armpits were identified and a straight line with an angle of 60° to the horizontal line defined two upper regions that were excluded. The region above the neck was excluded also. Figure 3a presents the result of this process.

The step of removing the lower border is the most critical in the segmentation process. Despite being a lighter region characterized by high temperature, the step is difficult because patients have different biotypes. The method for selecting borders begins in the central region and continues downward to each external region, excluding each pixel and its entire line below if:

. it has a value greater than or equal to $maxline - (1/max)$, where $maxline$ is the maximum value of the vertical line to which the pixel belongs, and max is the global maximum value;

. it has already had its most central neighbor excluded.

The result of excluding the lower border is shown in Figure 3b. In cases where the contrast of the image is very low, identifying the lower border is problematic and may result in a large loss of the ROI.

The last stage of segmentation was to remove possible residual upper lateral regions, by defining straight lines from the outer point of the lateral part of the image and forming 60° to the horizontal. The final segmented image is displayed in grayscale corresponding to the first equalization to make the visual comparison with the original image more natural (Figure 3c).

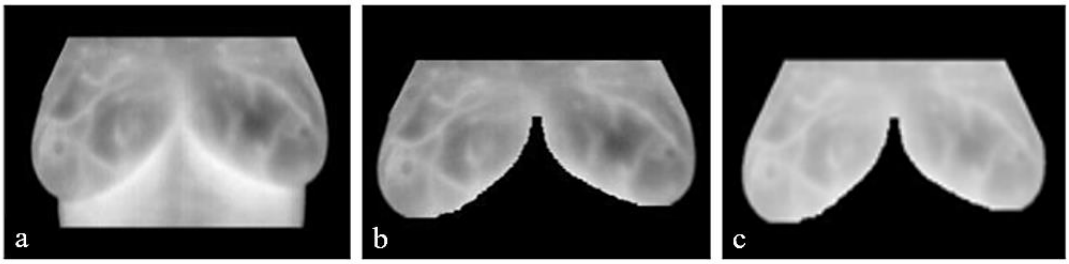

Figure 3. Results of the automatic segmentation steps. (a) Segmentation after determining the upper and lower limits and removing the residual upper lateral regions. (b) Image after removal of the border and lower region. (c) Final segmented image.

Ellipses manually generated by Matlab® are used in the manual segmentation. They are adapted to the breast by changing their dimensions, allowing the better control over the selected area. At the end of the process, two independent temperature matrices were obtained, one for the left (LB) and one for the right breast (RB) (Figure 4).

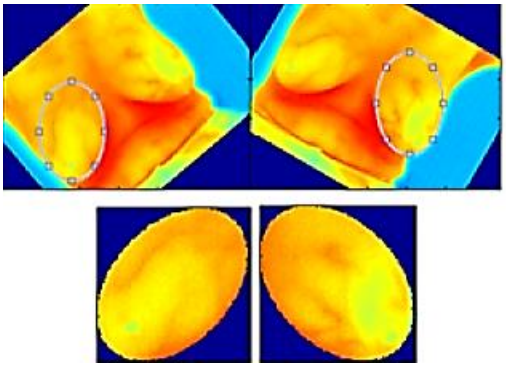

Figure 4. Results of the manual segmentation for two different patients.

Feature extraction

Twenty features related to breast temperature were extracted from segmented images after automatic segmentation. These features are based on statistical measures (such as mean, standard deviation and histograms analysis) and interval measures. A feature pair was selected using the free software WEKA ranker (Information Gain) to improve classifier performance and decrease the computational cost.

The extracted features are listed in Table 1. $\mathbf{T}_{min,RB}$ and $\mathbf{T}_{min,LR}$, $\mathbf{T}_{max,RB}$ and $\mathbf{T}_{max,LR}$ represent the minimum and maximum temperatures of the right breast (RB) and the left breast (LB), respectively. The features marked with an * are like the previous ones and are part of a set that considered pixels immediately below the inframammary borders.

The combination of c_3 with c_1^* was selected as the one that generated the most appropriate discrimination between classes, providing a smaller dispersion of these classes.

To extract features from manually segmented images, the extraction of interval features defined by Araújo et al. (2014) was used. Thus, interval characteristics were extracted from both the segmentation matrix (**S**) and the matrix **M** obtained through the morphological process.

The morphological process was carried out on the temperature values of the image, instead of the common transformation on the amplitude of their pixels. Given **T1** a temperature matrix i × j and T2 an structuring element radius n pixel, the morphological process was based on the following steps: a) Erosion in T1(ε_{T2}(**T1**)): Move T2 through all elements x_{ij} of **T1** and assign to x_{ij} the minimum value of temperature in the domain

defined by T2. b) Dilation in $\varepsilon_{T2}(\mathbf{T1})$ ($\delta_{T2}(\varepsilon_{T2}(\mathbf{T1}))$: Move T2 through all the elements x_{ij} of $\varepsilon_{T2}(\mathbf{T1})$ and associate with x_{ij} the maximum temperature value in the domain defined by T2, defining an approximate background value of **T1** ($\gamma_{T2}(\mathbf{T_1})$). c) Subtract the approximate background value $\gamma_{T2}(\mathbf{T_1})$) from the original temperature matrix **T1**, obtaining the morphological matrix (Araújo et al., 2014).

In an infrared image, the temperature range can be defined from the temperatures contained in the region of interest. An interval can be written as $y = [T_{min}, T_{max}]$, where T_{min} represents the minimum temperature and T_{max}, the maximum temperature. Thus, each input matrix gives rise to an interval variable, generating a four-dimensional interval feature vector $y = [v_1, v_2, v_3, v_4]$ where: $v_1 = \left[min_{\boldsymbol{S}_{RB}}, max_{\boldsymbol{S}_{RB}}\right]$, $v_2 = \left[min_{\boldsymbol{S}_{LB}}, max_{\boldsymbol{S}_{LB}}\right]$, $v_3 = [min\ (\boldsymbol{S}_{RB}, \boldsymbol{S}_{LB}), max(\boldsymbol{S}_{RB}, \boldsymbol{S}_{LB})]$ and $v_4 = \left[min\left\{max_{\boldsymbol{M}_{RB}}, max_{\boldsymbol{M}_{lB}}\right\}, max\left\{max_{\boldsymbol{M}_{RB}}, max_{\boldsymbol{M}_{lB}}\right\}\right]$.

Table 1. List of features.

Feature Number	Feature
$\mathbf{c_1}$	$\max\left(T_{max,RB}, T_{max,LB}\right)$
$\mathbf{c_2}$	$\min\left(T_{max,RB}, T_{max,LB}\right)$
$\mathbf{c_3}$	$\max\left(T_{min,RB}, T_{min,LB}\right)$
$\mathbf{c_4}$	$\min\left(T_{min,RB}, T_{min,LB}\right)$
$\mathbf{c_5}$	$c_1 - c_2$
$\mathbf{c_6}$	$c_2 - c_3$
$\mathbf{c_7}$	$c_3 - c_4$
$\mathbf{c_8}$	$c_1 - c_4$
$\mathbf{c_9}$	Mean of the temperature matrix
$\mathbf{c_{10}}$	Standard deviation of the temperature matrix
$\mathbf{c_{11}}$	Skewness of the histogram of temperatures
$\mathbf{c_{12}}$	Kurtosis of the histogram of temperatures
$\mathbf{c_1^*}$	$\max\left(T_{max,RB}, T_{max,LB}\right)$
$\mathbf{c_2^*}$	$\min\left(T_{max,RB}, T_{max,LB}\right)$
$\mathbf{c_3^*}$	$\max\left(T_{min,RB}, T_{min,LB}\right)$
$\mathbf{c_4^*}$	$\min\left(T_{min,RB}, T_{min,LB}\right)$
$\mathbf{c_5^*}$	$c_1^* - c_2^*$
$\mathbf{c_6^*}$	$c_2^* - c_3^*$
$\mathbf{c_7^*}$	$c_3^* - c_4^*$
$\mathbf{c_8^*}$	$c_1^* - c_4^*$

Then, each interval vectors v_n (n = 1, 2, 3, 4) was separated into two components: center and radius, generating two new continuous vectors. Briefly, given an interval observation y = [*a; b*], where *a* represents the maximum value, and *b*, the minimum value of the range, the center and radius are scalar values calculated using the Eqsuations (1) and (2), respectively.

$$center_y = (a + b)/2 \tag{1}$$

$$radius_y = (a - b)/2,\ \text{radius} \geq 0 \tag{2}$$

These vectors were transformed into a new feature space by Fisher's criterion. In this case, the individual samples were projected into a new feature space where these samples can be more easily separated (Webb & Copsey, 2011).

The output of this step is two-dimensional vectors for the centers (x_c) and for the radii (x_r). These vectors were coupled and a new interval vector $\dot{\mathbf{v}}$ was obtained as follows:

$$\dot{\mathbf{v}} = [x_c - x_r, x_c + x_r] \tag{3}$$

The characteristics above were selected for the development of the computational graphical interface. Each feature extraction was associated with its respective segmentation.

Classification processes

Thereafter, the selected variables served as input to classifiers used by the present study. The initial objective was to evaluate the performance of classifiers to analyze the database for the absence or presence of abnormalities (benign tumor, malignant tumor, and cyst). The methodology developed in this study adapted the classifiers to be used in individual patient's evaluation, which was not done previously by the two authors cited. Regarding the study by Araújo et al. (2014), the database was expanded, and the healthy class was included in the analysis.

Given a training base formed by several records (x_i, y_i), where x_i represents the vector of characteristics and y_i indicates the class that each vector belongs to, the classification problem is to construct a function/model containing a compact and functional description of the provided data. This function/model is used to classify new records whose classes are not known in advance.

Based on the analysis by Dourado Neto (2014), automatic segmentation was associated with the Support Vector Machine (SVM) with polynomial kernel. The SVM is a supervised learning method that performs well in pattern recognition problems. In addition, it has an extensive literature showing good results with the classification of thermographic images of the breast.

The distances evaluated by Araújo et al. (2014) for the minimum distance classifier were the Euclidean distance, the Mahalanobis distance and the City-Block distance. The minimum distance classifier calculated by the Mahalanobis distance parameterized presented better results and, therefore, was applied here with ROI manual extraction.

The parameterized Mahalanobis distance can be defined by a common covariance matrix between the lower and upper limits of the interval, parameterized for each class $q = 1,2,3,4$. Thus, considering $\lambda_q \in [0,1], (q = 1,2,3,4)$ as a control parameter for class C_q, a parameterized Mahalanobis distance between two interval vectors can be defined as

$$d^{\lambda}(\dot{\mathbf{v}}_t, \dot{\boldsymbol{g}}_{\boldsymbol{q}}) = \left(\mathbf{v}_{\mathrm{iI}} - \mathbf{g}_{q\mathrm{I}}\right)^T \mathbf{S}_q \left(\mathbf{v}_{\mathrm{iI}} - \mathbf{g}_{q\mathrm{I}}\right) + \left(\mathbf{v}_{\mathrm{iS}} - \mathbf{g}_{qS}\right)^T \mathbf{S}_q \left(\mathbf{v}_{\mathrm{iS}} - \mathbf{g}_{qS}\right) \quad (4)$$

where $\mathbf{S}_q(\lambda_q)(q = 1,2,3,4)$ represents the parameterized covariance matrix. The λ_q parameter measures the degree of relevance between the limits of the lower and upper intervals of the interval variables in the calculation of the parameterized covariance matrix of the class (Araújo et al., 2014).

Then, the performance of classifiers was analyzed to define the optimal parameters: polynomial kernel for the SVM, and λ_q for the parameterized Mahalanobis distance.

To determine the λ_q, an iterative process with increments of 0.1 and with λ_q ranging from 0 to 1 was implemented. Values of all weight parameters, corresponding to each class, were combined and the best combination chosen was the one whose total accuracy and sensitivity for the malignant class were the highest. Similarly, the polynomial kernel of the SVM classifier was determined by an iterative process ranging from 2 to 8 with increment of 1.

Both methods were evaluated by the cross-validation leave-one-out criterion, in which 97 patients (training group) were used to create the classification rule and a patient was used as a test. This evaluation was repeated for the 98 patients, until 98 different groups were used as training group and 98 different elements were used as test.

For individual analysis, codes of classification systems were adjusted so that the operator can select the image of the single patient and classify it. Thus, the image does not need to be in a specific directory, facilitating the storage process.

Two different groups were defined for both classifiers: the training group and the test group. The training group was formed by characteristics of the thermographic image database, and it was used in algorithm learning. And the test group will be each new patient classified in an unsupervised manner

Results and discussion

This section describes the results obtained using the SVM and Mahalanobis classifiers. Furthermore, the GUI-CAD ANALISE IR_MAMA created and its application in the analysis of test images was described.

Quantitative analysis of CAD systems

In this study, the IR image dataset was split into four classes: 20 healthy patients, 27 patients with benign tumors, 27 patients with malignant tumors and 24 patients with cysts. Initially, the SVM classifier, with polynomial kernel 8, and the Mahalanobis classifier were used for this sample. Table 2 lists the results of this process. Based on the results presented, the SVM classifier reached an accuracy of 74.49%, a sensitivity of 59.26% and a specificity of 83.82%. The Mahalanobis classifier had an accuracy of 41.84%, sensitivity of 92.59% and specificity of 35.55%.

The accuracy rate of the SVM classifier was higher than that of the Mahalanobis classifier. On the other hand, the sensitivity to Malignant Class using the Mahalanobis classifier was 33.33% higher than that obtained by the SVM classifier. The value related to the Processing Time of the program corresponds to the time interval between the beginning and end. In this case, the SVM classifier was three times faster than the Mahalanobis classifier.

The two CAD systems discussed so far were adjusted to run the classification process for a single patient, comparing their result with the results of the dataset. The CAD systems were implemented in a graphical user interface for greater applicability in aiding the diagnosis of breast cancer.

Table 2. Confusion matrix for the (a) SVM classifier (b) Mahalanobis classifier.

		Predicted				
		Malignant Tumor	Benign Tumor	Cyst	Healthy	Total
True	Malignant Tumor	16	3	0	8	27
	Benign Tumor	5	21	0	1	27
	Cyst	3	0	19	2	24
	Healthy	3	0	0	17	20

(a)

		Predicted				
		Malignant Tumor	Benign Tumor	Cyst	Healthy	Total
True	Malignant Tumor	25	0	0	2	27
	Benign Tumor	13	5	9	0	27
	Cyst	9	3	10	2	24
	Healthy	7	6	6	1	20

(b)

The graphical interface

This section presents the developed graphical interface and its application in the analysis of five random and independent patients with defined diagnoses:

. Patient 1: healthy breast;
. Patient 2: benign tumor;
. Patient 3: cyst;
. Patient 4 and Patient 5: malignant tumor.

The tests were performed in a computer with Windows 10 operating system, Intel Core i3 - 3217U (1.80 GHz), 4 GB RAM and 64-bit Operating System.

The adapted CAD systems were associated with a graphical user interface (GUI), created in the Matlab® platform, to make the process more automated. The use of an interface or framework allows the operator to use different techniques without prior knowledge of the software programming language. ANALISE IR_MAMA is a computational tool aid that allows the user to have an automated diagnosis for breast pathologies, based on the processing of infrared images. This software enables the individual analysis and classification of a patient by comparing with the database considered. The user can select the type of image segmentation - manual or automatic, in addition to other options and the choice of characteristics. All these options can be selected using a simple and intuitive GUI. Figure 5 illustrates the GUI that was developed. It has two menus (File and Help) and four panels (Patient Information, Segmentation, Results and Statistics).

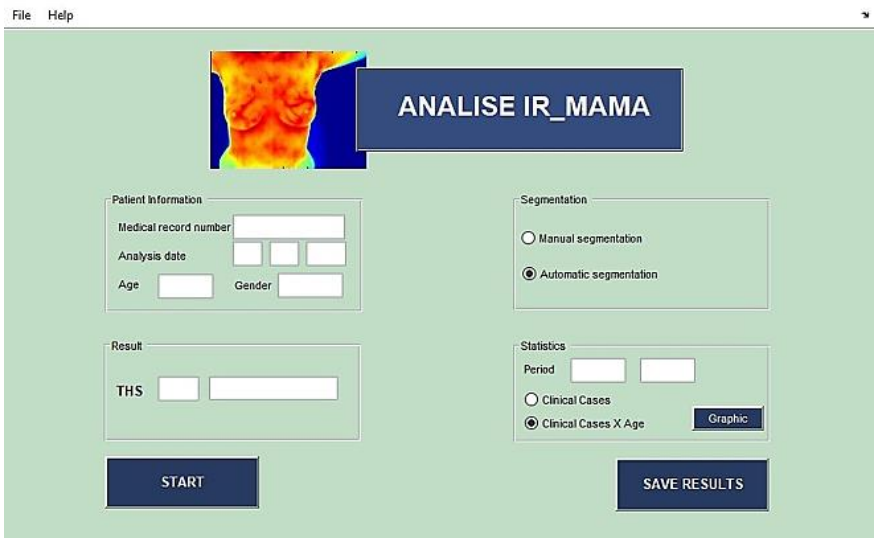

Figure 5. GUI ANALISE IR_MAMA.

In the File menu, the user has the option to open the IR image using the FLIR QuickReport program, and can export the temperature matrix in a .csv format or exit the interface. The Help menu presents a short explanation of the computational interface and functionalities.

In the Patient Information panel, the physician/researcher can insert the patient data, such as medical record number, age, and gender (male/female). Data are then stored in a .txt file so that they can be used subsequently in the Statistics panel.

In the Segmentation panel, the user can choose between two types of breast segmentation (manual or automatic), which are internally associated with the classifiers related to each type of segmentation.

The Statistics panel performs for a quantitative analysis of data recorded in each period. of data recorded in each period. For example, if the user wants to know the number of clinical cases (healthy patients, patients with malignant tumors, patients with benign tumors or patients with cysts) in 2015, for example, in the Period, the user should select up to 2015 and when the button Clinical Cases is pressed, a pie chart with the results will appear. Similarly, if the user wants to know the distribution of clinical cases according to patient's age, the user should select the Clinical Cases × Age button and histograms will appear for each class.

To standardize the results, a new THS index (Thermal Statistical Index) was defined, and it is based on IR images and the statistical classifiers to indicate the existence of possible breast pathologies. The proposal of this index is to be similar to the stratification of malignancy risk propose by BI-RADS, which is used in mammography and ultrasound exams.

The result associated with THS is displayed in the Result panel. In the first space a number between 1 and 4 will appear, referring to the index, and the second space will show the evaluation, according to the table above.

Finally, the classification is started when the Start button is selected. When the Save Results button is selected, the thermographic image of each patient will be saved as well as their data: medical records, diagnosis, and date of IR analysis.

Case study

In this topic, some applications of the graphical user interface: ANALISE IR_MAMA are presented. The patients' IR images do not belong to the fixed database, and they belong to patients diagnosed as healthy, with cyst, with benign tumor and with malignant tumor. Images were classified by the SVM and the Mahalanobis classifiers. Table 3 lists the results obtained.

To exemplify, a case of a patient with malignant tumor (invasive ductal carcinoma) is presented. The patient was 35 years old, and her diagnosis was completed through clinical examination, ultrasonography, mammography, and biopsy.

Figure 6 shows the results of the segmentation of the ROIs of the digital thermographic image. The automatic segmentation (Figure 6c) again presented problems in detecting the lower borders of the breasts, but this did not influence the extraction of the region of interest. The duration of the automatic segmentation process was 1.63s and the manual segmentation, 45.39s.

The result provided by the framework, using both classifiers, was a positive true (Malignant Tumor), because the patient was classified with the presence of a malignant tumor and in fact, she had it. The result of other analyses is presented in Table 3. In this table, the sensitivity shows the accuracy of the Malignant Tumor category, while the specificity is related to global matches to Non-cancer category, in other words, Benign Tumor, Cyst and Healthy.

This study is relevant by adopting the classification of breast thermograms into four classes (healthy, cyst, benign tumor, and malignant tumor). The method adopted for individual classification of breast thermographic images also stands out. This may be one of the major contributions of our approach.

In diagnosis systems, it is desirable to have high sensitivity and high specificity, but this is often not possible. Higher sensitivity leads to less specificity and vice versa. In tumor diagnosis, greater sensitivity is more important, because it supports the early detection of malignancy. Thus, the sensitivity of 92.59% achieved by the Mahalanobis classifier can be used as an aid in tracking patients with possible malignant lesions. The SVM classifier, which reached 83.82% specificity with fast processing time, can be useful to confirm the patient's individual result in clinical screening.

The GUI created proved to be efficient in its proposal and can be easily used by specialists as an auxiliary tool in analysis. The friendly aspect of interface can help the physician to classify a patient without prior knowledge of classifiers details.

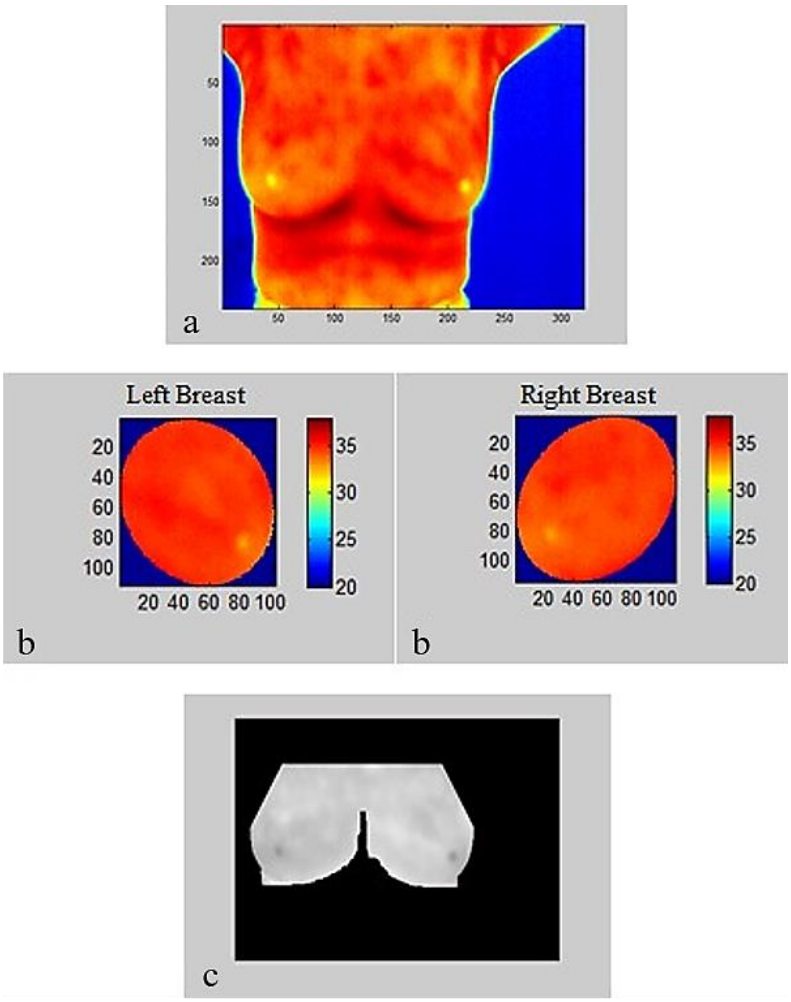

Figure 6. Patient's segmentation. (a) Thermographic image. (b) Manual segmentation. (c) Automatic segmentation.

able 3. Results obtained for the classification of patients analyzed.

Patients	Age	Diagnosis	SVM	Mahalanobis
Patient 1	35	Malignant Tumor	THS 4	THS 4
Patient 2	52	Healthy	THS 1	THS 2
Patient 3	38	Cyst	THS 1	THS 4
Patient 4	42	Benign Tumor	THS 3	THS 1
Patient 5	57	Malignant Tumor	THS 3	THS 4

Although the general complementary accuracy of classifiers tested in this study was lower than in some studies found in the literature (Table 4), it is possible to notice how the isolated sensitivity and isolated specificity of the Mahalanobis and SVM classifiers are close to or greater than the results of other authors. Thus, the combined test of these classifiers would be of great value. The combined test intends to increase the positive predictive value of a positive result in the initial test. This is possible through the combination of two classifiers. The classifiers are used consecutively, the second is applied only if the first one yields a positive result. Thus, the Mahalanobis classifier would be used for screening and, in case of a positive result for cancer, the SVM classifier would be applied to confirm the diagnosis. The test result will be considered positive if both tests are positive.

The present study has some limitations. Although there is no single method that works well for all problems with unbalanced data, the sampling methods showed potential as they try to improve the dataset, prior to classification. In general, the subsampling methods, applied in this study, are characterized by dataset balance through the elimination of majority instances. The limitation of this method is the possibility of removing majority instances that carry important information from the sample, especially in cases where the dataset is small. In addition, the database used in this study was predominantly composed of women over 55

years old and it is known that the current limitation of mammography focuses on the low application for dense breasts (women aged 18 to 25 years). Thus, the low quantitative of thermograms of women with dense breasts is also a limitation.

Table 4. Synthesis of breast thermographic image classification results of studies cited in this work.

Author	Database	Classifier	Accuracy (%)	Sensitivity (%)	Specificity (%)
Araújo et al. (2014)	14 M 19 B 17 C	Mahalanobis distance	84.00	85.70	86.50
Dourado Neto (2014)	43 M 79 B 42 C 70 H	SVM	89.36	87.50	90.32
Ahmed et al. (2019)	43 M 45 B 30 H	SVM	97.14	98.00	98.60
Santana et al. (2018)	235 M 371 B 219 C	ELM	71.22	–	–
Vasconcelos et al. (2018)	41 M 47 B 46 C 41 H	SMO	63.46	80.77	86.54
Rodrigues et al. (2019)	76 M 121 B 73 C 66 H	SVM	91.12	–	–
Present study	27 M 27 B	SVM	74.49	59.26	83.82
	24 C 20 H	Mahalanobis distance	41.84	92.59	35.55

*M = Malignant tumor; B = Benign tumor; C = Cyst; H = Healthy

Conclusion

This study presented a new computational tool to aid in the detection of breast abnormalities using thermographic images. Such tool added efficient and simple options for segmentation (automatic and manual) of thermographic images of the breast, as well as a multi classification of mammary pathologies. With the presented tool, it was possible to conduct analysis of a single patient, reaching a sensitivity of 92.59%.

Based on those considerations, it is especially expected that the use of thermography combined with a mammary dysfunction analysis tool can help in the early diagnosis of breast cancer, being efficient for previous screening.

References

Acharya, U. R., Ng, E. Y. K., Sree, S. V., Chua, C. K., & Chattopadhyay, S. (2014). Higher order spectra analysis of breast thermograms for the automated identification of breast cancer. *Expert Systems: The Journal of Knowledge Engineering, 31*(1), 37–47. DOI: https://doi.org/10.1111/j.1468-0394.2012.00654.x

Ahmed, A. A., Ali, M. A. S., & Selim, M. (2019). Bio-inspired based techniques for thermogram breast cancer classification. *International Journal of Intelligent Engineering & Systems, 12*(2), 114–124. DOI: https://doi.org/10.22266/IJIES2019.0430.12

Araújo, M. C., Lima, R. C. F., & Souza, R. M. C. R. d. (2014). Interval symbolic feature extraction for thermography breast cancer detection. *Expert Systems with Applications, 41*(15), 6728–6737. DOI: https://doi.org/10.1016/j.eswa.2014.04.027

Araújo, M. C., Souza, R. M. C. R., Lima, R. C. F., & Silva Filho, T. M. d. (2017). An interval prototype classifier based on a parameterized distance applied to breast thermographic images. *Medical & Biological Engeneering & Computing, 55*(6), 873–884. DOI: https://doi.org/10.1007/s11517-016-1565-y

Bezerra, L. A., Oliveira, M. M., Araújo, M. C., Viana, M. J., Santos, L. C., Santos, F. G., ... Conci, A. (2013). Infrared imaging for breast cancer detection with proper selection of properties: from acquisition

protocol to numerical simulation. In E. Y. K. Ng, U. R. Acharya, R. M. Rangayyan & J. S. Suri (Eds.), *Multimodality Breast imaging: Diagnosis and Treatment* (Vol. 1, p. 285-332). Bellingham, DC: SPIE Press. DOI: https://doi.org/10.1117/3.1000499

Dourado Neto, H. M. (2014). *Automatic segmentation and analysis of thermograms: an auxiliary method for the detection of breast cancer* (master's thesis). Federal University of Pernambuco, Recife, Pernambuco.

Duffy, S. W., Tabár, L., Yen, A. M.-F., Dean, P. B., Smith, R. A., Jonsson, H., ... Chen, T. H.-H. (2020). Mammography screening reduces rates of advanced and fatal breast cancers: results in 549,091 women. *Cancer, 126*(13), 2971–2979. DOI: https://doi.org/10.1002/cncr.32859

Ekici, S., & Jawzal, H. (2020). Breast cancer diagnosis using thermography and convolutional neural networks. *Medical Hypotheses, 137*, 109542. DOI: https://doi.org/10.1016/j.mehy.2019.109542

Instituto Nacional de Câncer José Alencar Gomes da Silva [INCA]. (2019). *Estimativas 2020: incidência de Câncer no Brasil*. Rio de Janeiro, RJ: INCA.

Kapoor, P., Prasad, S. V. A. V., & Patni, S. (2012). Image segmentation and asymmetry analysis of breast thermograms for tumor detection. *International Journal of Computer Applications, 50*(9), 40–45. DOI: https://doi.org/10.5120/7803-0932

Rodrigues, A. L., Santana, M. A. d., Azevedo, W. W., Bezerra, R. S., Barbosa, V. A. F., Lima, R. C. F. d., & Santos, W. P. d. (2019). Identification of mammary lesions in thermographic images: feature selection study using genetic algorithms and particle swarm optimization. *Research on Biomedical Engineering, 35*(3-4), 213–222. DOI: https://doi.org/10.1007/s42600-019-00024-z

Santana, M. A. d., Pereira, J. M. S., Silva, F. L. d., Lima, N. M. d., Sousa, F. N. d., Arruda, G. M. S. d., ... Santos, W. P. d. (2018). Breast cancer diagnosis based on mammary thermography and extreme learning machines. *Research on Biomedical Engineering, 34*(1), 45–53. DOI: https://doi.org/10.1590/2446-4740.05217

Singh, D., & Singh, A. K. (2020). Role of image thermography in early breast cancer detection- past, present, and future. *Computer Methods and Programs in Biomedicine, 183*, 105074. DOI: https://doi.org/10.1016/j.cmpb.2019.105074

Sung, H., Ferlay, J., Siegel, R. L., Laversanne, M., Soerjomataram, I., Jemal, A., ... Bray, F. (2021). Global cancer statistics 2020: GLOBOCAN estimates of incidence and mortality worldwide for 36 cancers in 185 countries. *CA: A Cancer Journal for Clinicians, 71*(3), 209–249. DOI: https://doi.org/10.3322/caac.21660

Vasconcelos, J. H. d., Santos, W. P. d., & Lima, R. C. F. d. (2018) Analysis of methods of classification of breast thermographic images to determine their viability in the early breast cancer detection. *IEEE Latin America Transactions, 16*(6), 1631–1637. DOI: https://doi.org/10.1109/TLA.2018.8444159

Webb, A. R., & Copsey, K. D. (2011). *Statistical pattern recognition* (3th ed.). New York, NY: Wiley.